Scalar dissipation modeling for passive and active scalars: *a priori* study using Direct Numerical Simulation

L. C. Selle[1] and J. Bellan[1,2]

[1] *California Institute of Technology*
[2] *Jet Propulsion Laboratory, California Institute of Technology*

Abstract

Transitional databases from Direct Numerical Simulation (DNS) of three-dimensional mixing layers for single-phase flows and two-phase flows with evaporation are analyzed and used to examine the typical hypothesis that the scalar dissipation Probability Distribution Function (PDF) may be modeled as a Gaussian. The databases encompass a singlecomponent fuel and four multicomponent fuels, two initial Reynolds numbers (Re), two mass loadings for two-phase flows and two free-stream gas temperatures. Using the DNS calculated moments of the scalar-dissipation PDF, it is shown, consistent with existing experimental information on single-phase flows, that the Gaussian is a modest approximation of the DNS-extracted PDF, particularly poor in the range of the high scalar-dissipation values, which are significant for turbulent reaction rate modeling in non-premixed flows using flamelet models. With the same DNS calculated moments of the scalar-dissipation PDF and making a change of variables, a model of this PDF is proposed in the form of the β-PDF which is shown to approximate much better the DNS-extracted PDF, particularly in the regime of the high scalar-dissipation values. Several types of statistical measures are calculated over the ensemble of the fourteen databases. For each statistical measure, the proposed β-PDF model is shown to be much superior to the Gaussian in approximating the DNS-extracted PDF. Additionally, the agreement between the DNS-extracted PDF and the β-PDF even improves when the comparison is performed for higher initial Re layers, whereas the comparison with the Gaussian is independent of the initial Re values. For two-phase flows, the comparison between the DNS-extracted PDF and the β-PDF also improves with increasing free-stream gas temperature and mass loading. The higher fidelity approximation of the DNS-extracted PDF by the β-PDF with increasing Re, gas temperature and mass loading bodes well for turbulent reaction rate modeling.

Keywords: scalar dissipation modeling

1. Introduction

In non-premixed turbulent combustion models it is often assumed that flames are infinitesimally thin with respect to turbulence scales, and thus that turbulence merely distorts these flames, thus increasing their surface and augmenting the reaction rate; these are called 'flamelet' models. In these simplified models, the turbulent reaction rate is assumed to be proportional to the scalar dissipation, which is specified through a

mathematical form. Typically, the PDF of scalar dissipation is assumed to be a Gaussian despite recent experimental evidence that in flows at engineering relevant Reynolds numbers (Re) this may not be a very good approximation.

The investigations of the last decade were primarily concentrated on analyzing the scalar dissipation in single-phase (SP) flows. Both experiments with liquid (i.e. $Sc = O(10^2)$ conditions) [1] and gaseous flows (i.e. $Sc = O(1)$ conditions) [3] were performed. Passive scalars have been previously studied [2]-[7] (in the [7] spray engine, the drops have a 4 ms stay in pressurized air, after which the resulting gas is injected in the measurement chamber) and [8]. Active, reactive scalars have also been investigated [9]-[14]. The relationship between scalar dissipation and strain in non-reacting turbulent planar jets at atmospheric pressure has also been addressed [6]. Some experimentalists [4] [8] concentrated on measuring the dissipation in propane jets (seeded with acetone) co-flowing with air. Others [9] [11]-[14] focussed on measuring the scalar dissipation for atmospheric methane/air jet flames; some evidence was shown [11] introducing skepticism about the applicability of flamelet concepts to those flames.

If one defines

$$\chi \equiv \mathcal{D}[(-\nabla(cX_v)) \cdot (-\nabla(cX_v))] \qquad (1)$$

where $\mathcal{D}$ is an effective (constant) diffusion coefficient defined as the proportionality coefficient between the vapor mass flux and $cm\nabla(X_v/m)$, c is the molar density, m is the molar mass (subscript v denotes the vapor), X is the mole fraction and $\rho = mc$ is the mass density, then the inquiry on the mathematical form of the scalar dissipation PDF translates into finding the mathematical form of the $\log(K)$ PDF, where $K = \chi/\mathcal{D}$. All experimental investigations of passive scalars, e.g. [1] [7] [8], show that the PDF of $\log(K)$ is indeed close to a Gaussian, but that it exhibits a small negative skewness that distinguishes it from the Gaussian (which has null skewness). The departure from Gaussian was shown [8] to hold at significant values and over an engineering-useful range of (outer scale) Re (3290 to 8330). When conditioned to larger Re, the skewness magnitude was reduced, consistent with lucid discussions [5] regarding the subtle departure from local isotropy for both inertial and dissipation scales at experimentally attainable values of (rather than infinite) Re and with considerations on the scalar PDF tails. However, for the Re magnitudes relevant to engineering applications, the non-Gaussian behavior prevails, as also experimentally found [11] for active scalars.

The scalar dissipation in two-phase (TP) flows remains virtually unaddressed despite its relevance to sprays and general heterogeneous combustion. Also, for both SP and TP flows there have been no attempts to inquire whether PDF forms other than Gaussian are better representations of the actual scalar-dissipation PDF. The present study palliates to these unfulfilled needs by systematically analyzing the scalar dissipation for a variety of realizations obtained under different conditions and by ultimately proposing a better representation of the actual scalar dissipation, particularly with increasing Re and gas temperatures where the flamelet model is justified. The flows analyzed are transitional states obtained from Direct Numerical Simulation (DNS).

2. Description of the conservation equations

The DNS equations have been presented in detail elsewhere [15]-[17] and thus only a succinct description is given here, the reader being referred to those extensive publications for particular information.

For SP flows, the DNS equations consist of the perfect-gas equation of state coupled to three-dimensional (3D) Eulerian conservation equations for mass, momentum, energy and species, each equation having transient, convection and diffusion terms. For TP flows, the gas-phase Eulerian equations are complemented with Lagrangian conservation equations following each physical drop in its trajectory as it changes mass, momentum, energy and (if relevant) species, due to its dynamic and thermodynamic interaction with the gas, here taken to be air. Because the drops are much smaller than the Kolmogorov scale, they can be treated as sources of mass, species, momentum and energy for the gas [18] (e.g. [19]). Thus, the interaction of the drops with the gas manifests as mass, species, momentum and energy source terms in the gas conservation equations, coupling thus the drops and gas. A geometric weighting factor distributes each drop contributions to the nearest eight grid points in proportion to its distance from the drop location. Because numerical diffusion induced by distributing the Lagrangian source terms at the Eulerian nodes is proportional to the ratio of the drop volume by the discretization volume, this potential effect is here negligible since this ratio is initially $O(10^{-3})$ and decreases with time as the drops evaporate. Although a model is used to describe the drops' behavior and thus the TP simulations are not strictly DNS, this terminology [20] has been adopted in the literature [15]-[19] and is also used here for consistency. The drop model has been experimentally validated [21].

For each TP simulation, the drops consist of either a singlecomponent (SC) or a multicomponent (MC) liquid having initially the same identity for all drops; for SC simulations, the liquid identity naturally remains the same for all drops during the calculations, however, for MC simulations each drop develops its own liquid composition according to its dynamic/thermodynamic history due to preferential evaporation of some species with respect to others. Thus, for SC simulations, the vapor partial density is sufficient to describe the gas composition because the mixture is vapor and air. However, for MC liquid drops, the information about the vapor partial density is complemented by the details of the composition both for the liquid and the evolving vapor due to evaporation.

The mathematical description of the composition for practical liquid fuels containing hundreds or thousands of species has been pioneered [22] using Continuous Thermodynamic (CT) concepts [23] [24]. In the CT theory the chemical potential for a mixture containing numerous components is appropriately represented, and the Gibbs function is derived through molecular thermodynamic methods in terms of the probability distribution function (PDF) describing the mixture composition. The concepts are fundamental and independent of the physicochemical model chosen for the chemical potential. Having specified an initial composition PDF, the evolution of the mixture is governed by thermodynamic relationships and/or conservation equations. Although the most general PDF will depend on many variables, it has been shown, with validation, that the single-Gamma PDF depending on m can represent a homologous species class [24] [25]. Single-Gamma PDF models applied to drop evaporation [22] have been shown [26] to be restricted to negligible fuel vapor in the drop-surrounding gas. A combination of two Gamma PDFs (DGPDF) as a function of m is necessary to capture the evaporation of drops in a gas containing substantial fuel vapor [26], as in sprays. Moreover, the DGPDF concept has been enlarged [27] through appropriate thermodynamic modeling and it was shown that a single DGPDF can represent several homologous species classes.

3. Results

3.1. Description of the databases

The DNS equations have been solved in a 3D temporal mixing layer of dimensions $(L_1 \times L_2 \times L_3)$ with (x_1, x_2, x_3) being the streamwise, cross-stream and spanwise directions, respectively (see Fig. 1 in [15]) for the conditions listed in Table 1 encompassing SP MC, TP SC and TP MC simulations. Perturbations were used to excite the layer in order to induce roll-up and pairing [15] [28]. For TP flows, initially, all the drops are in the lower stream and have the same temperature, $T_{d,0}$ (subscript 0 denotes initial condition), which is lower than both the initial gas temperature T_0 and the liquid boiling point temperature to promote evaporation; the initial velocity of each drop is the same as that of the gas phase at its location. The drop size distribution is specified through the Stokes number $St = \tau_d \Delta U_0 / \delta_{\omega,0}$, as given as in Table 1; $\Delta U_0 = 2U_0$ is the initial velocity difference across the layer with $U_0 = M_{c,0}\sqrt{R_a T_0 C_{p,a}/C_{v,a}}$ where $M_{c,0}$ is the convective Mach number, $R_a = R_u/m_a$ where R_u is the universal gas constant and subscript a denotes the carrier gas (here air), C_p and C_v are constant-pressure and constant-volume heat capacities, $\tau_d = \rho_l D^2/(18\mu)$ is a characteristic drop time constant where D is the drop diameter and μ is the gas viscosity, and $\delta_{\omega,0}$ is the initial vorticity thickness calculated as in [15]. The specified value of $\mathrm{Re}_0 = \rho_0 \Delta U_0 \delta_{\omega,0}/\mu$ is used to calculate μ. The thermal conductivity and diffusivity are computed using this value of μ and specified values of Prandtl, Pr, and Schmidt, Sc, numbers ($\mathrm{Pr} = Sc$, 0.696 at $T_0 = 375$ K and 0.694 at $T_0 = 400$ K [21]). The initial number of drops, N_0, is determined by the initial mass loading ML_0 (initial ratio of liquid mass to mass of carrier gas in drop-laden part of domain). For all TP simulations, the vapor molar fractions in the lower stream, $X^l_{v,0}$, and upper stream, $X^u_{v,0}$, are here specified $X^l_{v,0} = X^u_{v,0} = 0$ for the SC fuel (n-decane) and 10^{-4} for MC fuels (an arbitrarily small non-null value is necessary to avoid instabilities). For each MC liquid, the free-stream vapor composition is found from a single-drop simulation in air at the specified T_0, being chosen to be the first-time-step surface-vapor composition. For SP MC simulations, $X^l_{v,0} = 10^{-1}$ and $X^u_{v,0} = 10^{-4}$ so as to create a vapor mass flux between the two streams; the value of 10^{-1} approximately corresponds to the average lower-stream value encountered at transitional states in TP simulations.

The boundary conditions in the (x_1, x_3) homogeneous directions were periodic and adiabatic slip-wall conditions derived for MC mixtures [16] were utilized in the x_2 direction. For TP flows, drops reaching the slip walls were assumed to stick to them.

The numerics consisted of an eighth-order central finite difference discretization in space and a fourth-order Runge-Kutta for temporal advancement. A fourth-order Lagrange interpolation was used to obtain gas-phase variable values at drop locations. Drops whose mass decreased below 3% of the initial mass were removed from the calculation; for all computations, mass was conserved in the system to a maximum relative error of $O(10^{-5})$. The time step was controlled by the CFL number. The grid size was chosen such that resolution was excellent as manifested by velocity-fluctuation-based one-dimensional energy spectra which showed no accumulation of energy at the small scales [15] [17]. Each simulation reached a transitional state, evidenced by a smooth energy spectrum except for a small peak at the perturbation frequency. It is the set of these transitional states that constitutes the present database.

The SC fuel was n-decane [15] and the MC fuels were diesel and three kerosenes (Jet A, RP-1 and JP-7) [17] whose composition [29] was provided by Edwards [30] and is shown elsewhere [16] as a Single-Gamma PDF. Thermodynamic and transport properties for these fuels are available [15]-[17].

3.2. Scalar dissipation visualizations

Displayed in Fig. 1 are contour plots of $\log_{10}(K)$ at transition for selected simulations. For SP simulations, cX_v is a passive scalar, however, for TP simulations it is an active scalar as it originates from phase change. In all cases, the known filamentary aspect of $\log_{10}(K)$ [8] is evident with regions of high and low values being adjacent. Comparing SP and TP flows at same initial conditions (Figs. 1f versus

1d and 1e) one detects higher local structure when $ML_0 \neq 0$, which is amplified with increasing ML_0 (Figs. 1a versus 1b; 1d versus 1e). This increased structure is also evident in comparisons of all realizations in Fig. 1 with Fig. 2 of [8] and is attributed to the drop/flow interaction. Basically, the vapor source terms locally increase X_v, thus generating higher gradients, a situation which is typical of TP flows. Increasing Re_0 also leads to more convoluted contours (Figs. 1a versus 1c), being the expected result of the increasing flow turbulence. At same specified initial conditions, the structure increases for diesel compared with n-decane (Figs. 1d versus 1a; 1e versus 1b) which is a manifestation of the longer evaporation time of diesel drops, promoting additional local drop/flow interactions, whereas the intensity is larger for n-decane than for diesel because of the larger n-decane evaporation rate. All kerosenes display less scalar-dissipation structure than diesel (not shown), this resulting from the shorter drop evaporation time. Finally, as T_0 increases, the structure of the scalar dissipation decreases as well (not shown), also owing to the more vigorous drop evaporation.

3.3. DNS-extracted versus Gaussian PDF

The PDFs were calculated either over $|x_2/\delta_{\omega,0}| < 4$ (domain denoted (ml-4)) so as to exclude the quiescent upper and lower streams (see Fig. 1) or over $|x_2/\delta_{\omega,0}| < 2$ (domain denoted (ml-2)) to further restrict the range of local Re to the highest values in the mixing layer. The first two moments of the DNS-extracted PDF in (ml-4) are listed in Table 2. All mean values are negatives indicating that $K \in [0,1]$; in fact, calculations show that $K \leqslant 10^{-1}$. Because larger absolute values of the PDF mean correspond to smaller mean of K, Table 2 shows for TP cases that with increasing Re_0 or ML_0 the mean of K is smaller but its standard deviation is larger, resulting from to the increased range of scales with both parameters. At same specified initial conditions, the mean of K is larger and the variance is smaller for n-decane than for the MC fuels, and the mean of K is larger for kerosenes than for diesel with no clear trend for the variance. Finally, at higher T_0, the mean of K is larger and so is its variance, indicating a more intricate flow structure. For SP flows, at the larger Re_0 the mean of K is not affected but its variance increases, which is again a manifestation of the increased range of flow scales.

Typical DNS-extracted PDFs of $\log_{10}(K)$ are presented in Fig. 2 along with the corresponding Gaussian calculated with the moments of the DNS-extracted PDF. Because the moments defining the Gaussian are exact, the comparison of Fig. 2 is exclusively devoted to the mathematical form of the PDF. Clearly, the Gaussian overestimates/underestimates the exact PDF in the largest/smallest scalar dissipation values regime, as particularly evident in the logarithmic-axis plots; while in between the extreme values, either overestimates or underestimates may occur both of which are enhanced at larger Re_0 or T_0 (not shown) or with higher fuel volatility, and which subside with increased ML_0. Evidently, there is a substantial discrepancy between the Gaussian and exact PDF, particularly at the largest scalar-dissipation values significant for flamelet modeling.

3.4. Proposed scalar dissipation PDF model

The shortcomings of the Gaussian PDF of $\log_{10}(K)$ prompt a reconsideration for the representation of the DNS-extracted PDF. Just as for the Gaussian PDF, we decouple here the two issues of PDF-moment modeling and PDF shape, and concentrate only on the latter by utilizing the DNS-calculated moments. That is, if we find a better than Gaussian model for the PDF shape, the outcome will be the best attainable model for that PDF given that under usual circumstances moment modeling will naturally introduce inaccuracies.

The shape of the DNS-extracted PDFs in Fig. 2 suggests exploring whether the β-PDF is a better choice than the Gaussian. However, while the Gaussian is defined over $\mathbb{R}$, the β-PDF is only defined for intervals in $\mathbb{R}^+$. A change of variables can palliate this potential problem and also provide a non-dimensionalization that facilitates comparisons among DNS-extracted, Gaussian and β PDFs. We define $\mathcal{A}$ as the ensemble of all values of $\log_{10}(K)$, $a \equiv \min_{\mathcal{A}}[\log_{10}(K)]$ and $b \equiv \max_{\mathcal{A}}[\log_{10}(K)]$. Then, with $XX \equiv [\log_{10}(K) - a]/[b-a]$ where $XX \in [0,1]$, and real numbers p and q

$$P_\beta[\log_{10}(K); p, q, a, b] \equiv \frac{\Gamma(p+q)}{\Gamma(p)\Gamma(q)} \times \frac{XX^{(p-1)}(1-XX)^{(q-1)}}{b-a} \quad (2)$$

$$= \frac{P_\beta(XX; p, q, 0, 1)}{b-a} \quad (3)$$

where P_β is the β-PDF whose mean is $[p/(p+q)]$ and variance is $\{pq/[(p+q)^2(1+p+q)]\}$, and where Γ is the Gamma function. The focus is now on PDFs of XX, postponing to further *a posteriori* studies the return to the $\log_{10}(K)$ PDF.

Plotted in Fig. 3 are DNS-extracted, Gaussian and β PDFs of XX for the same simulations as in Fig. 2. Evidently, $P_\beta(XX; p, q, 0, 1)$ is a much better representation of the exact PDF than the Gaussian, especially in the range of high XX where $\log_{10}(K)$ has large values; inherently, the Gaussian does not have the mathematical form of the exact PDF, independent of the system of coordinates.

Results obtained for all simulations emulate those of Fig. 3. To quantify the departures of the Gaussian and β PDFs from the corresponding DNS-extracted PDF, several statistical tests were performed over the ensemble of all simulations, and these results are listed in Table 3. Three ensembles of DNS-extracted PDFs were considered: (ml-4), (ml-2), and (ml-4)$\cup$(ml-2). One test calculated the maximum absolute

difference, another computed the absolute mean difference and yet another the r.m.s. A useful statistics is the Kolmogorov-Smirnov test that measures the absolute difference, K-S, between two cumulative distribution functions [31]; its usefulness consists in the fact that if two data sets are drawn from the same distribution, the distribution of the statistics can be calculated, which gives the significance of the non-null value of K-S. Finally, the least-square fit constant and the correlation were also calculated. A cursory look at Table 3 indicates that because for each statistics type the standard deviation is smaller than the mean, all mean values are statistically significant. A closer examination shows that all statistics are consistent in that the β-PDF is superior to the Gaussian in representing the DNS-extracted PDF. The most dramatic comparison is that of the absolute mean difference where over (ml-4) both mean and standard deviation are smaller for the β-PDF by 4 orders of magnitude compared with those of the Gaussian; over (ml-2) and (ml-4)$\cup$(ml-2) the mean and standard deviation are smaller for the β-PDF by about 3 orders of magnitude compared with the Gaussian. The least dramatic statistics are the correlation and least-square fit which show comparable (but still superior for the β-PDF) results both for the mean and (with two exceptions) for the standard deviation (a smaller standard deviation makes the mean result more significant).

4. Conclusions

Transitional databases from DNS of single-phase multicomponent flows and evaporating two-phase flows of either singlecomponent or multicomponent fuel type were utilized to analyze the scalar dissipation. These transitional databases were obtained from calculations of 3D mixing layers; although the databases do not represent fully turbulent and/or combustion cases, variation trends with increasing Re, source strength for active scalars and initial gas temperature project the results validity to the turbulent combustion realm. Scalar-dissipation contour plots displayed the filamentary aspect found in experiments and exhibited a high degree of convolution and structure which increased with increasing initial mass loading of the drops, with decreased fuel volatility, and with decreased initial gas temperature. PDFs of the DNS-extracted scalar dissipation were calculated both over the mixing layer excluding the free streams and over an even more restricted part of the mixing layer representing its core. In all cases a Gaussian calculated using the moments of the DNS-extracted scalar dissipation displayed erratic agreement with the exact PDF over most of the range of scalar product values, with underestimates for the very small values, which are of limited interest, and overestimates for the very large values that are of paramount interest in flamelet models. An inquiry into better models than the Gaussian showed that within a new system of scalar-dissipation coordinates, the β-PDF calculated with the exact moments is a much superior representation of the DNS-extracted PDF, particularly in the regime of large scalar dissipation values. Six types of statistics were performed over the ensemble of the DNS realizations to quantify the departure of either Gaussian or β-PDF from the DNS-extracted PDF. Each statistics confirms the visually observed superiority of the β-PDF over the Gaussian.

Acknowledgments

This study was conducted at the Jet Propulsion Laboratory (JPL), California Institute of Technology (Caltech), under the partial sponsorship of the Donors of The Petroleum Research Fund administered by the American Chemical Society through a grant (to JB) for Caltech Post Doctoral Fellow (LS) support and of the U.S. Department of Energy. Computational resources were provided by the supercomputing facility at JPL.

References

[1] K. A. Buch, W. J. A. Dahm, *J. Fluid Mech.*, 317 (1996) 51-71.

[2] C. Tong, Z. Warhaft, *J. Fluid Mech.* 292 (1995)1-38.

[3] K. A. Buch, W. J. A. Dahm, *J. Fluid Mech.*, 364 (1998) 1-29.

[4] L. K.Su, N. T. Clemens, *Exp. In Fluids*, 27 (1999) 507-521.

[5] Z. Warhaft, *Annu. Rev. Fluid Mech.* , 32 (2000)203-240.

[6] P. S. Kothnur, N. T. Clemens, 2001 Experimental investigation of the relationship between strain and scalar dissipation in gas-phase turbulent jets. AIAA 2001-1023.

[7] D. M. Probst, J. B. Ghandi, *Int. J. Engine Res.*, 4(1) (2003) 27-45.

[8] L. K. Su, N. T. Clemens, *J. Fluid Mech.*, 488 (2003) 1-29.

[9] A. N. Karpetis, R. S. Barlow, *Proc. Comb. Inst.* 29 (2002) 1929-1936.

[10] S. D. Mason, J. H. Chen, H. G. Im, *Proc. Comb. Inst.*, 29 (2002)1629-1636.

[11] A. N. Karpetis, R. S. Barlow, *Proc. Comb. Inst.* 30 (2005) 663-670.

[12] R. S. Barlow, A. N. Karpetis, *Proc. Comb. Inst.* 30 (2005) 671-678.

[13] R. S. Barlow, A. N. Karpetis, *Flow, Turbulence and Combustion* 72 (2004) 427-448.

[14] A. N. Karpetis, T. B. Settersten, R. W. Schefer, R. S. Barlow, *Optics Letters*, 29(4) (2004)355-357.

[15] N. Okong'o, J. Bellan, *J. Fluid Mech.*, 499 (2004)1-47.

[16] P. C. Le Clercq, J. Bellan, *J. Fluid Mech.*, 533, (2005) 57-94; 540, (2005)439.

[17] L. C. Selle, J. Bellan, Direct numerical simulation of transitional multicomponent-species gaseous and multicomponent-liquid drop-laden mixing layers, submitted, 2005

[18] M. Boivin, O. Simonin, K. D. Squires, *J. Fluid Mech.*, 375 (1998)235-263.

[19] F. Mashayek, *J. Fluid Mech.*, 367 (1998)163–203.

[20] K. D. Squires, J. K. Eaton, *Phys. Fluids A*, 3 (1991) 1169-1178.

[21] R. S. Miller, K. Harstad, J. Bellan, *Int. J. Multiphase Flow*, 24 (1998)1025-1055.

[22] W. L. H. Hallett, *Combust. Flame*, 121 (2000)334-344.

[23] B. Gal-Or, H. T. Cullinan, Jr., R. Galli, *Chem. Eng. Sci.*, 30 (1975)1085-1092.
[24] R. L. Cotterman, R. Bender, J. M. Prausnitz, *Ind. Eng. Chem. Process Des. Dev*, 24 (1985)194–203.
[25] G. F. Chou, J. M. Prausnitz, *Fluid Phase Equilibria*, 30 (1986)75-82.
[26] K. G. Harstad, P. C. Le Clercq, J. Bellan, *AIAA J.*, 41(10) (2003)1858-1874.
[27] K. G. Harstad, J. Bellan, *Comb. Flame*, 137(1-2) (2004)163-177.
[28] R. D. Moser, M. M. Rogers, *Phys. Fluids A*, 3 (1991) 1128–1134.
[29] T. Edwards, L. Q. Maurice, *J. Comp. Phys.*, 17 (2001) 461-466.
[30] T. Edwards, private communication, (2002).
[31] W. H. Press, B. P. Flannery, S. A. Teukolsky, W. T. Vetterling, *Numerical recipes. The art of scientific computing.*, Cambridge University Press, 1989,p. 472-475.

Case	fuel	T_0	ML_0	ρ_l	Re_0	$X^l_{v,0}$	$\{\{D_0\}\}$ $\times 10^5$	N_0 $\times 10^{-3}$
dec375ML2R5	decane	375	0.2	642	500	$X^u_{v,0}$	8.600	2993
dec375ML2R6	decane	375	0.2	642	600	$X^u_{v,0}$	8.600	2993
dec375ML5R5	decane	375	0.5	642	500	$X^u_{v,0}$	8.600	7480
die375ML0R5	diesel	375	0	NA	500	10^{-1}	NA	NA
die375ML0R6	diesel	375	0	NA	600	10^{-1}	NA	NA
die375ML2R5*	diesel	375	0.2	828	500	$X^u_{v,0}$	7.601	2586
die375ML5R5	diesel	375	0.5	828	500	$X^u_{v,0}$	7.601	6451
die400ML2R5	diesel	400	0.2	828	500	$X^u_{v,0}$	7.359	2670
jetA375ML2R5	Jet A	375	0.2	800	500	$X^u_{v,0}$	7.732	2543
jetA400ML2R5	Jet A	400	0.2	800	500	$X^u_{v,0}$	7.487	2626
rp1375ML2R5	RP-1	375	0.2	800	500	$X^u_{v,0}$	7.732	2600
rp1400ML2R5	RP-1	400	0.2	800	500	$X^u_{v,0}$	7.487	2626
jp7375ML2R5	JP-7	375	0.2	800	500	$X^u_{v,0}$	7.732	2541
jp7400ML2R5	JP-7	400	0.2	800	500	$X^u_{v,0}$	7.487	2626

Table 1: Initial conditions. T_0 in K, ρ_l in kg/m^3, D_0 in m. In all simulations, $M_{c,0}$=0.35, $\delta_{\omega,0}$=6.859$\times 10^{-3}$m, $\{\{St_0\}\}$=3 and $\{\{(St_0 - \{\{St_0\}\})^2\}\}^{1/2}$=0.5, the double curly brackets denoting drop-ensemble averaging. $T_{d,0}$=345K, $X^u_{v,0} = 0$ for n-decane and $X^u_{v,0} = 10^{-4}$ for all MC fuels. For n-decane and $\mathrm{Re}_0 = 500$ the grid is 256$\times$288$\times$160, and for $\mathrm{Re}_0 = 600$ the grid is 288$\times$320$\times$176. For all MC fuels and $\mathrm{Re}_0 = 500$ the grid is 360$\times$400$\times$216 and for $\mathrm{Re}_0 = 600$ the grid is 432$\times$480$\times$260. The baseline case is indicated by a superscript asterisk. The n-decane and the jetA375ML2R5 simulations were performed on a SGI Origin 2000 platform (on 64, R12000, 300MHz processors); dec375ML2R5 was performed on the same Origin but on 32 processors; all other simulations were conducted on a SGI Altix 3000 machine (on 32, Intel Itanium2, 900MHz processors).

Case	mean	variance
dec375ML2R5	-3.19	6.17×10^{-1}
dec375ML2R6	-3.23	6.31×10^{-1}
dec375ML5R5	-3.20	6.48×10^{-1}
die375ML0R5	-4.22	7.95×10^{-1}
die375ML0R6	-4.22	9.34×10^{-1}
die375ML2R5	-3.82	6.83×10^{-1}
die375ML5R5	-3.68	7.53×10^{-1}
die400ML2R5	-3.63	7.02×10^{-1}
jetA375ML2R5	-3.43	6.86×10^{-1}
jetA400ML2R5	-3.25	7.03×10^{-1}
rp1375ML2R5	-3.51	6.77×10^{-1}
rp1400ML2R5	-3.29	7.17×10^{-1}
jp7375ML2R5	-3.47	6.78×10^{-1}
jp7400ML2R5	-3.25	7.19×10^{-1}

Table 2: First two moments of the $\log_{10}(K)$ DNS-extracted PDF in $|(x_2/\delta_{\omega,0})|<4$.

			maxd	meand	r.m.s.	K-S	ls	corr
(ml-4)	mean	G-PDF	3.2×10^{-1}	1.4×10^{-3}	1.2×10^{-1}	1.9×10^{-2}	9.973×10^{-1}	9.958×10^{-1}
		β-PDF	2.7×10^{-1}	1.1×10^{-6}	8.5×10^{-2}	1.2×10^{-2}	9.997×10^{-1}	9.978×10^{-1}
	std. dev.	G-PDF	1.7×10^{-1}	6.2×10^{-4}	6.0×10^{-2}	9.3×10^{-3}	4.198×10^{-3}	4.328×10^{-3}
		β-PDF	1.0×10^{-1}	6.3×10^{-7}	3.2×10^{-2}	5.0×10^{-3}	4.983×10^{-3}	1.819×10^{-3}
(ml-2)	mean	G-PDF	3.3×10^{-1}	1.4×10^{-3}	1.2×10^{-1}	2.0×10^{-2}	9.956×10^{-1}	9.950×10^{-1}
		β-PDF	2.6×10^{-1}	2.4×10^{-6}	8.2×10^{-2}	1.2×10^{-2}	9.999×10^{-1}	9.976×10^{-1}
	std. dev.	G-PDF	1.6×10^{-1}	9.3×10^{-4}	5.9×10^{-2}	9.5×10^{-3}	5.333×10^{-3}	5.741×10^{-3}
		β-PDF	8.2×10^{-2}	1.2×10^{-6}	3.4×10^{-2}	6.0×10^{-3}	5.217×10^{-3}	2.346×10^{-3}
(ml-2)	mean	G-PDF	3.3×10^{-1}	1.4×10^{-3}	1.2×10^{-1}	2.0×10^{-2}	9.964×10^{-1}	9.954×10^{-1}
$\cup$		β-PDF	2.6×10^{-1}	1.8×10^{-6}	8.3×10^{-2}	1.2×10^{-2}	9.998×10^{-1}	9.977×10^{-1}
(ml-4)	std. dev.	G-PDF	1.6×10^{-1}	7.8×10^{-4}	5.9×10^{-2}	9.3×10^{-3}	4.790×10^{-3}	5.006×10^{-3}
		β-PDF	9.2×10^{-2}	1.2×10^{-6}	3.4×10^{-2}	5.4×10^{-3}	5.008×10^{-3}	2.065×10^{-3}

Table 3: Statistics, both mean and standard deviation (std. dev.), of the Gaussian and β PDFs deviations from the DNS-extracted PDF of XX calculated over the ensemble of databases of Table 1. "maxd"= maximum absolute difference; "meand"= absolute mean difference; "r.m.s."= root mean square of the absolute difference; "K-S" = Kolmogorov-Smirnov test; "ls"= least square fit constant; "corr"= correlation. "ml-4" and "ml-2" signify that the DNS-extracted PDFs were calculated over $|(x_2/\delta_{\omega,0})|<4$ or $|(x_2/\delta_{\omega,0})|<2$, respectively.

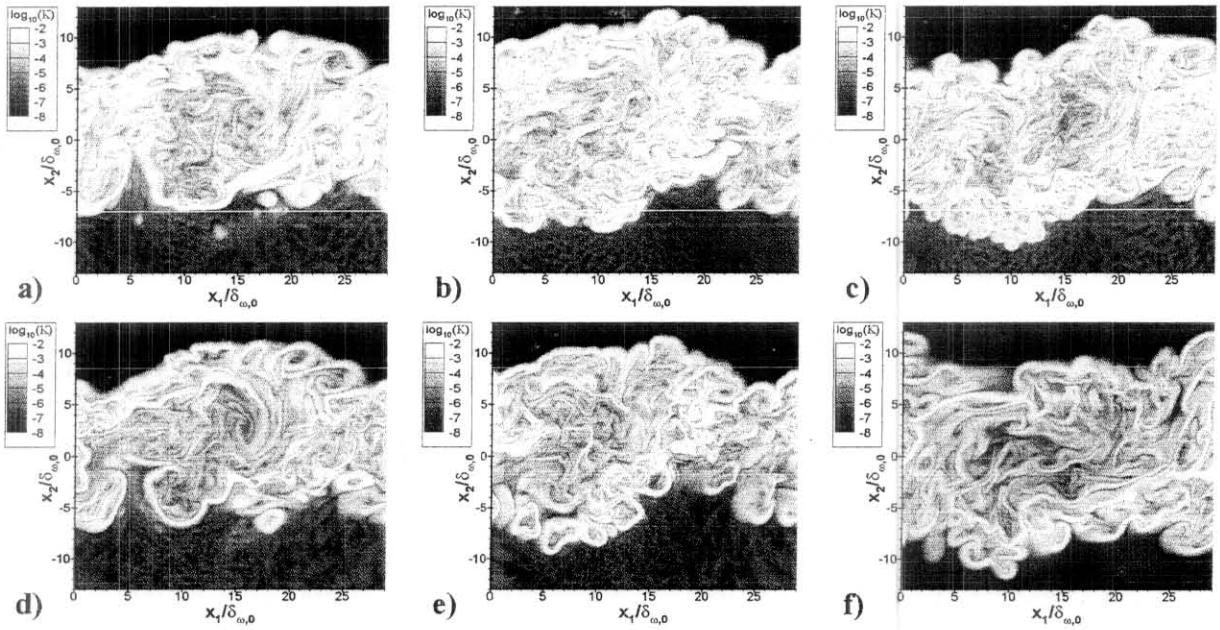

Fig. 1: Contour plots of $\log_{10}(K)$ in the between-the-braid plane $x_3/L_3 = 0.5$ for a) dec375ML2R5, b) dec375ML5R5, c) dec375ML2R6, d) die375ML2R5, e) die375ML5R5, and f) die375ML0R5.

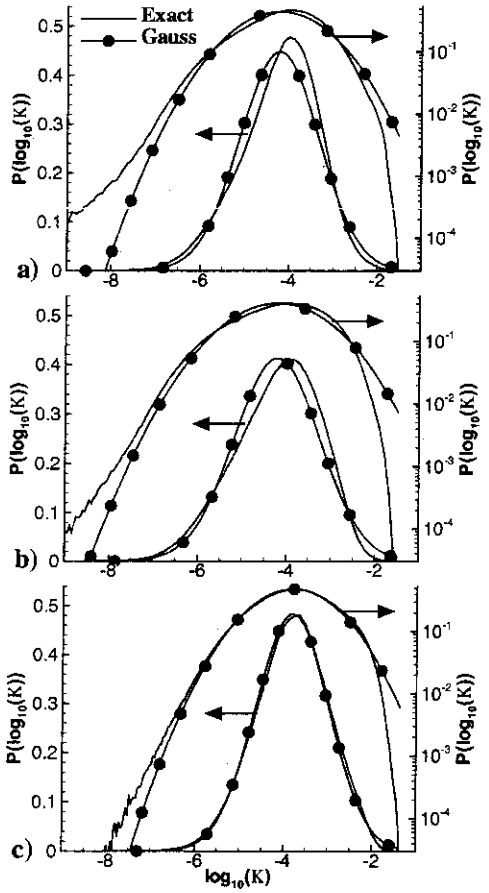

Fig. 2: DNS-extracted PDF of $\log_{10}(K)$ and Gaussian PDF constructed with the moments of the DNS-extracted PDF over $|x_2/\delta_{\omega,0}| < 4$. a) die375ML0R5, b) die375ML0R6 and c) die375ML2R5.

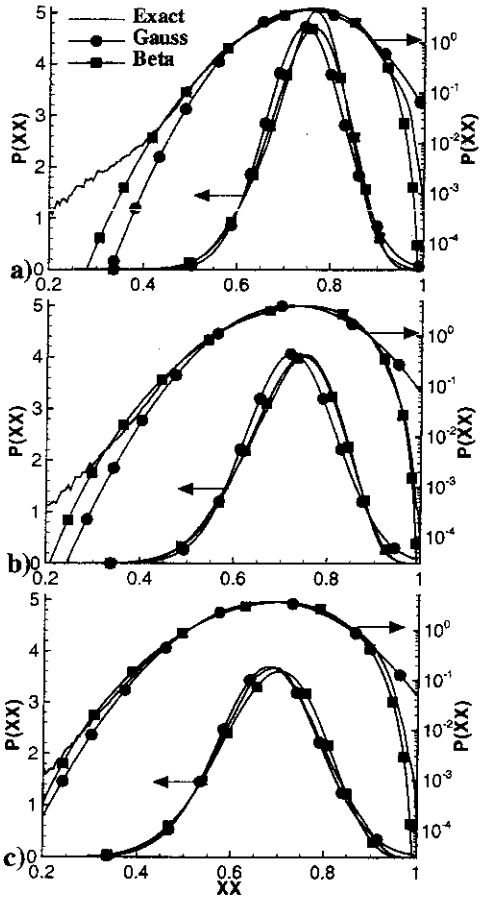

Fig. 3: DNS-extracted PDF of XX, and Gaussian and β PDFs constructed with the moments of the DNS-extracted PDF calculated over $|x_2/\delta_{\omega,0}| < 4$. a) die375ML0R5, b) die375ML0R6 and c) die375ML2R5.